Influence of Sand-Grain Morphology and Iron-Oxide Distribution Patterns on the Visible and Near-Infrared Reflectance of Sand-Textured Soils

Gladimir V. G. Baranoski, *Senior Member*, *IEEE*, Bradley W. Kimmel, T. Francis Chen, and Erik Miranda

***Abstract*—The overall shape of a sand grain can be defined by two morphological properties, namely sphericity and roundness, and it is largely determined by soil-formation and weathering processes. In this paper, we investigate the effects of these properties on the visible and near-infrared reflectance of sand-textured soils characterized by the presence of iron oxides. Our investigation is supported by computer simulations performed using the SPLITS (*S*pectral *L*ight *T*ransport Model for *S*and) model and considering actual sand characterization data. Our findings indicate that the influence of grain morphology may vary considerably depending on the distribution patterns of iron oxides present in sand-textured soils. These minerals may occur as pure particles, as contaminants mixed with the grain parent material, or as coatings. Since these distribution patterns are also significantly affected by soil-formation and weathering processes, we believe that the combined influence of sand-grain shape and iron-oxide distribution patterns on the reflectance of sandy landscapes should be carefully taken into account in the retrieval of information about their mineralogy and environmental history.**

***Index Terms*—Iron oxide, morphology, reflectance, roundness, sand, shape, simulation, sphericity, transportation, weathering.**

I. Introduction

THE spectral reflectance of sandy landscapes, such as dune fields found in deserts, coastal regions, and inland areas originally occupied by lake or sea beds, is significantly affected by the size and shape of their constituent grains as well as the presence of iron oxides (e.g., hematite, goethite, and magnetite). These minerals may occur as pure particles [1], as contaminants mixed with the parent material (e.g., quartz) [2], or as coatings within a kaolinite or illite matrix [3]. These morphological and mineralogical characteristics, in turn, are directly associated with the different formation processes of these sand-textured soils (Fig. 1), notably through wind or water transport [3]–[5]. Accordingly, their spectral signature can be employed to infer information about their mineralogy and environmental history [6], [7]. Moreover, the integration of this spectral data with computer modeling techniques can also lead to the accurate prediction of future changes in sandy terrains [8].

Manuscript received October 15, 2013; accepted December 31, 2013. Date of publication January 29, 2014; date of current version November 04, 2014. This work was supported in part by the Natural Sciences and Research Council of Canada (NSERC) under NSERC Grant 238337.

The authors are with the Natural Phenomena Simulation Group (NPSG), David R. Cheriton School of Computer Science, University of Waterloo, Waterloo, ON N2 L 3G1, Canada (e-mail: gvgbaran@cs.uwaterloo.ca).

Color versions of one or more of the figures in this paper are available online at http://ieeexplore.ieee.org.

Digital Object Identifier 10.1109/JSTARS.2014.2299813

Previous remote sensing works in this area have focused on the effects of grain size on the reflectance of sand-textured soils [7], [9], [10]. In addition, when computer simulations are employed to investigate these effects, the grains are often represented by perfect spheres [7], [9], [11]. However, it has been suggested that not only size variations, but also shape variations need to be taken into account in investigations linking the spectral signature of sand-textured soils to their formation processes and mineralogical characteristics [1], [3], [5], [12], [13].

The overall shape of a sand grain can be defined in terms of two main properties: sphericity (or eccentricity) and roundness (or angularity) [14]–[16]. While the former refers to the degree to which a grain approaches a spherical shape, the latter refers the curvature of its corners and edges [12] and it is associated with the large-scale roughness (or smoothness) of its surface [17], [18]. The small-scale roughness of a sand grain, on the other hand, is associated with its surface's micro-texture [17], [18], which can be masked by the presence of iron-oxide coatings [19], [20].

Transportation of sand grains either by wind or water may involve rolling, suspension, and saltation [14], a processs in which the grains are temporarily suspended by the wind before impacting the sand soil surface [21], [22]. Accordingly, sphericity and roundness properties are directly connected to the formation history of a sand deposit as well as the immediate conditions at the site of deposition [12]. For example, particles with high sphericity roll faster than particles with low sphericity [14]. Similarly, particles with low sphericity may also behave differently from particles with high sphericity during suspension since the ratio of the surface area to the volume of a particle is directly associated with its response to lifting forces [12]. Moreover, the roundness of the corners and edges may indicate the rigor of the last stage of transportation [16]. Increasing rigor increases fracturing and chipping, which, in turn, may increase sphericity and reduce roundness [14].

Roundness can also be affected by abrasion and solution processes [14], [17]. While the former reduces roundness, the later increases it. A high degree of roundness is often an indicator of gentle conditions of wear and it is usually observed in sand deposits formed through gentle tractional transportation [16]. Hence, water-transported grains tend to have much smoother and uncoated surfaces than wind-transported (aeolian) grains due to continuous dissolution processes [3], [21]. Aeolian grains, on the other hand, tend to have rougher surfaces due to the saltation process.

In this paper, which is an extended and updated version of a conference presentation [23], we investigate how variations in

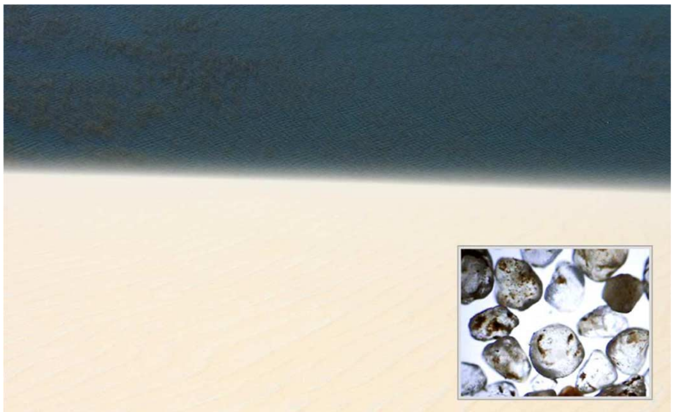

Fig. 1. Photograph showing a coastal sandy landscape affected by wind and water transport processes. Inset: microscope photograph depicting sand grains with distinct iron-oxide contents.

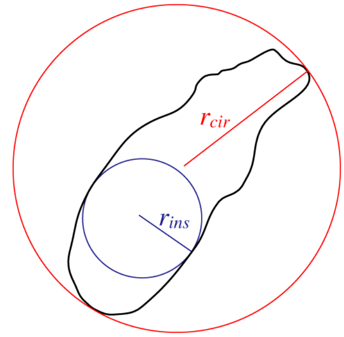

Fig. 2. Projection of a sand grain onto a plane used in the computation of Riley sphericity [27]. The radii r_{ins} and r_{cir} correspond to the radius of the largest inscribed and the radius of the smallest circumscribed circles, respectively.

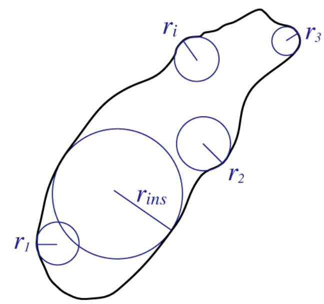

Fig. 3. Projection of a sand grain onto a plane used to compute its roundness using Wadell's method [14], [16]. The radii r_{ins} and r_i correspond to the radius of the largest inscribed circle and the radius of curvature of a particle corner i, respectively.

the sphericity and roundness of sand grains may alter the visible and near-infrared spectral signature of sandy landscapes characterized by distinct iron-oxide distribution patterns. Iron oxides, such as hematite, magnetite, and goethite, can have a strong influence in the visible and near-infrared reflectance of sand-textured soils [1], [9], [10]. In fact, the presence of these minerals can be used to map the distribution of nutrients and heavy metals in these soils on the basis of the surface reflectance of these terrains [6]. Although this work focus on roundness and sphericity properties, it also includes observations related to grain size. Our investigation is based on *in silico* controlled experiments performed using a predictive simulation set-up and supported by actual sand measured data. Within this set-up, we assign different values to specific parameters, particularly those associated with the size, sphericity, and roundness of the sand grains, and analyze their spectral effects while keeping the other parameters constant. It is worth nothing that such controlled experiments are usually difficult to be performed under actual laboratory conditions [6], [13], [24].

The remainder of this paper is organized as follows. In Section II, we outline morphological concepts and definitions relevant for this work. In Section III, we briefly describe the simulation framework employed in our investigation. In Section IV, we present the baseline spectral datasets used in our simulations. In Section V, we report our findings and discuss their theoretical and practical implications. Finally, in Section VI, we close the paper and outline directions for future research in this area.

II. Morphological Concepts and Definitions

Soil grains are divided into three classes, or soil separates, namely sand, silt, and clay, from the largest to the smallest particles, respectively [25]. The relative masses of each soil separate are compared to determine the texture of a soil sample. A sand-textured soil, henceforth referred to as sand soil, contains at least 85% sand-sized particles.

Different methods can be used to quantify the roundness (R) and the sphericity (S) of a sand particle. The sphericity values considered in this work were obtained by Vepraskas and Casel [26] using the sphericity measure proposed by Riley [27]. Its definition is based on the projection of the particle onto a plane and it is given by

$$S = \sqrt{\frac{r_{ins}}{r_{cir}}} \tag{1}$$

where r_{ins} and r_{cir} correspond to the radius of the largest inscribed circle and the radius of the smallest circumscribed circles, respectively, as shown in Fig. 2. Note that a sphere has a sphericity equal to 1.

The roundness values considered in our investigation were also obtained by Vepraskas and Casel [26]. They employed a method for assessing grain roundness that consists in visually comparing images of individual grains to images of grains of varying roundness depicted in reference charts [24], [28]. These charts are derived from the Krumbein chart [12], which contains images of grains with a known roundness computed using the method proposed by Wadell [14]. According to Wadell [14]–[16], the roundness of a sand grain can be quantified as the average radius of curvature of the N grain corners relative to the radius of the maximum sphere that can be inscribed in the grain [14]. This quantification can be expressed as

$$R = \frac{\sum_{i=1}^{N} \frac{r_i}{N}}{r_{ins}} \tag{2}$$

where r_i corresponds to the radius of curvature of a corner i as shown in Fig. 3. Note that a sphere has a roundness equal to 1.

III. Simulation Framework

The modeled directional-hemispherical reflectance curves depicted in this work were computed using the SPLITS (*Sp*ectral *Li*ght *T*ransport Model for *S*and) model [29]. This model employs Monte Carlo methods and ray optics techniques to simulate light interactions with individual sand grains distributed in the pore medium (air or water). SPLITS can be run online via a model dissemination framework [30] that enables researchers to specify simulation parameters (e.g., angle of incidence, spectral range, and sand characterization data) through a web interface (Fig. 4), and receive customized simulation results via e-mail. Hence, researchers can fully reproduce our results and extend our investigation to other experimental conditions. It is worth noting that although SPLITS provides bidirectional readings, one can obtain directional-hemispherical quantities [31] (provided by our online system [32]) by integrating the outgoing light (rays) with respect to the collection hemisphere [33], [34]. Similarly, bihemispherical quantities can be calculated by integrating the bidirectional scattering distribution function (BDF) values with respect to the incident and collection hemispheres [29]. For completeness, in this section, we briefly review aspects of the SPLITS formulation that are directly related to the main theme of our investigation, and outline the datasets used in our simulations. We remark that a detailed description of the SPLITS model can be found elsewhere [29].

The SPLITS model takes into account the individual morphological characteristics of the sand grains. More specifically, their sphericity and roundness are normally distributed, with their mean and the standard deviation derived from data provided by Vepraskas and Cassel [26], and constrained to fall within their respective ranges derived from the same data (Table I). Their size, represented by their diameter D is distributed according to a piecewise log-normal distribution as suggested by Shirazi *et al.* [25], i.e., $\log D$ is normally distributed. This distribution is characterized by two parameters, namely the geometric mean particle diameter d_i and its standard deviation σ_i, which are functions of the soil texture. That is, the percentages of the sand-sized, silt-sized, and clay-sized particles are employed to compute the respective geometric mean diameters and standard deviations of these particles (Table II) using a particle size distribution provided by Shirazi *et al.* [25].

Within the SPLITS formulation, an individual particle consists of a core and an optional coating. The core represents the grain parent material, which in terrestrial sand soils is typically a material like quartz or calcite, with quartz (employed in this investigation) being the most common [9]. The core is modeled as a prolate spheroid with a semiminor axis a and a semimajor axis c. The length of c is given by $D/2$, while the length of a is given by $c * S^2$. It is also worth noting that SPLITS is not limited to the use of prolate spheroids. Optionally, the core may be coated by a mineral layer whose thickness h is proportional to the particle size, i.e., $h = Dh'$, where h' is the relative coating thickness. The relative coating thickness, in turn, is given by $h' = h_r/D_r$, where h_r and D_r correspond to the coating reference thickness and the coating reference diameter, respectively. These reference parameters are derived from coating data provided in the literature [3]. We remark that the coating layer consists of iron oxides embeded in a kaolinite (employed in this investigation) or illite matrix.

The interfaces between the core, coating, and surrounding medium are modeled using randomly oriented facets of equal area to simulate a rough surface. The orientations of these facets are distributed such that the dot product between the facet normal n' and the interface normal n is given by $n' \cdot n = 1 - |X|$, where X is normally distributed with zero mean and standard deviation given by $(1 - R)/2$. This standard deviation was chosen so that $R < n' \cdot n \leq 1$ for 95% of the facets [29]. Additionally, the facet normals are constrained so that $n' \cdot n > 0$. Hence, the particle roundness is used to control the large-scale roughness of the interfaces and, consequently, the spatial distribution of the light interacting with them.

IV. Baseline Spectral Datasets

As the baseline references for our investigation, we computed modeled reflectance curves (over the 400–1000 nm region) for four selected sand samples with distinct mineralogical characteristics whose reflectance curves were measured by Rinker *et al.* [35]. These measured curves were made available in the U.S. Army Topographic Engineering Center (TEC) database [35]. These sand samples are originally from a red (hematite-rich) dune in Australia (TEC #10019201), a dune in Saudi Arabia (TEC #13j9823), a magnetite-rich site in Peru (TEC #10039240), and a dike outcrop in California (TEC #19au9815). Based on their descriptions [35], we assumed that the presence of clay-sized particles, organic matter, and water (moisture) were negligible in these samples. Besides the parameters associated with the shape and size of the particles (Tables I and II), the mean values used for porosity (42.5% [36]) and the relative coating thickness ($5\ \mu\text{m}/1.2\ \text{mm}$ [37]) were also obtained from data provided in the literature. The remaining parameter values employed to compute the modeled spectral reflectance curves for these samples are given in Table III.

In the measurements performed by Rinker *et al.* [35], reflected radiance is collected from the normal direction and compared to the reflected radiance of a white reference sample. Based on the experimental set-up described by Rinker *et al.* [35], we inferred that the illumination geometry may be appropriately represented using a hemispherical light source. The measured data provided by Rinker *et al.* [35] is thus in the form of a hemispherical-directional reflectance factor [39]. It is important to note, however, that the hemispherical-directional reflectance factor is mathematically equivalent to the directional-hemispherical reflectance [39]. We remark that this radiometric quantity, in turn, can be computed by casting rays from an angle of incidence equal to 0° and collecting all rays reflected into the upper hemisphere using a virtual spectrophotometer [33].

As it can be observed in the graphs presented in Fig. 5, the modeled curves show a close agreement with their measured counterparts, specially considering that we employed the same average values for key model input parameters such as porosity, coating thickness, roundness, and sphericity. Besides the visual inspection of the modeled curves, we also computed the root-mean-square errors (RMSEs) with respect to their measured counterparts: 0.0172, 0.0166, 0.0095, and 0.0120 for the

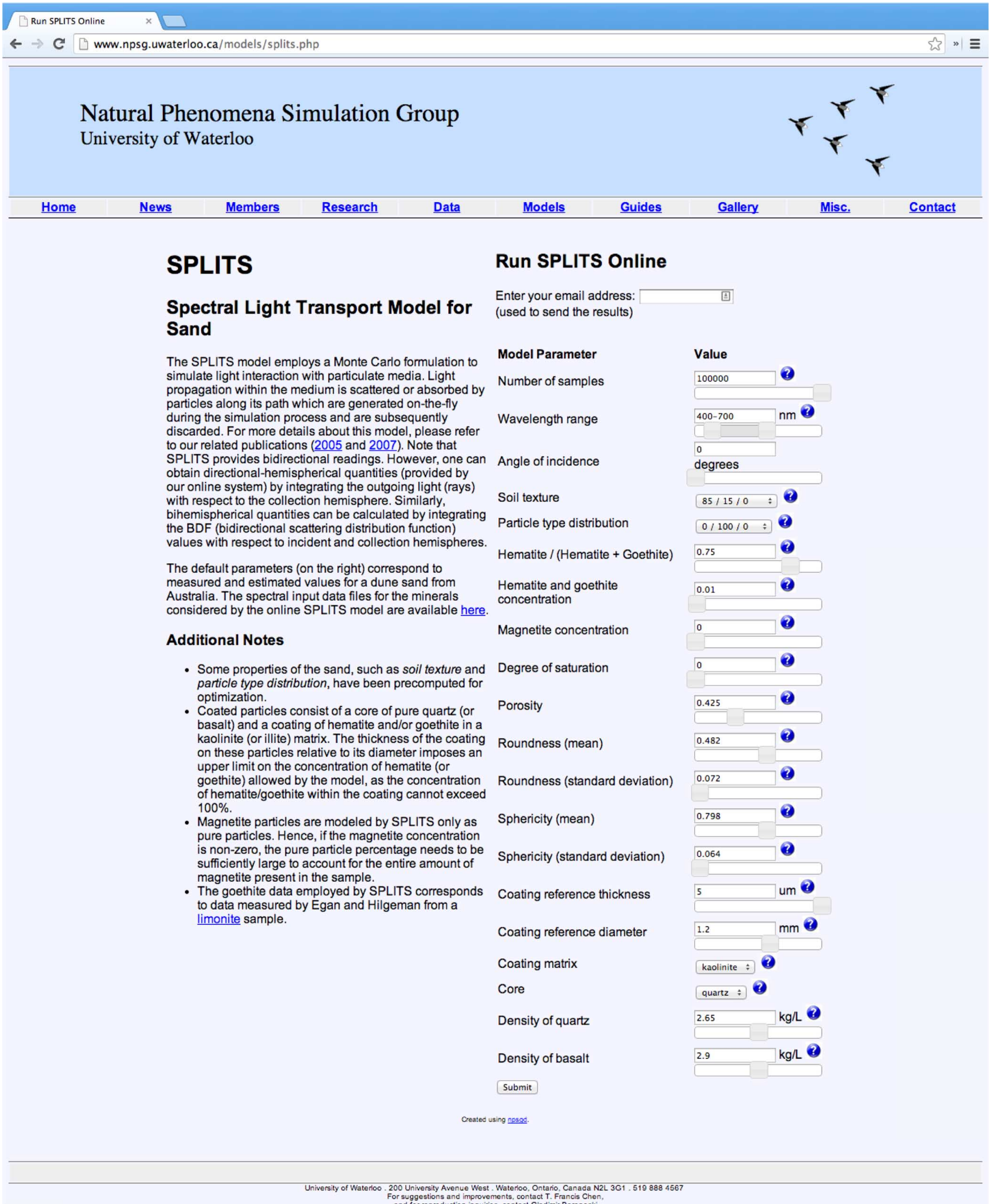

Fig. 4. Web interface for the SPLITS model available through the Natural Phenomena Simulation Group Distributed (NPSGD) framework [30]. Through this web interface [32], researchers can configure physical parameters and execute light transport simulations involving different sand samples.

Australian, Saudi, Peruvian, and Californian samples, respectively. These RMSE values below 0.03 (the empirical value usually associated with good spectral reconstruction [40]) further indicate a good agreement between the modeled and measured curves. Accordingly, we employed these modeled curves as the control (baseline) curves in our *in silico* experiments, which

TABLE I
MEAN, STANDARD DEVIATION AND RANGE VALUES FOR SPHERICITY AND ROUNDNESS PROVIDED BY VEPRASKAS AND CASSEL [26]

	Mean	Standard deviation	Min	Max
Roundness	0.482	0.072	0.2	0.7
Sphericity	0.798	0.064	0.6	0.95

TABLE II
GEOMETRIC MEAN PARTICLE DIAMETERS (GIVEN IN MM) AND STANDARD DEVIATIONS FOR SOILS WITH VARIOUS MIXTURES OF SAND-SIZED PARTICLES (s_1) AND SILT-SIZED PARTICLES (s_2) CONSIDERED IN OUR SIMULATIONS

Fractions		Sand		Silt	
s_1	s_2	d_1	σ_1	d_2	σ_2
0.850	0.150	0.112	2.170	0.173	3.320
0.900	0.100	0.129	2.090	0.272	3.750
0.928	0.072	0.141	2.040	0.401	4.160
0.950	0.050	0.155	1.990	0.640	4.720
1.000	0.000	0.316	0.164	–	–

The diameters and standard deviations for sand-sized particles (d_1 and σ_1, respectively) and silt-sized particles (d_2 and σ_2, respectively) are provided by Shirazi *et al*. [25]. Note that the presence of clay-sized particles is assumed to be negligible in the sand samples considered in this work.

TABLE III
PARAMETERS USED TO OBTAIN THE MODELED SPECTRAL REFLECTANCE CURVES FOR THE AUSTRALIAN, PERUVIAN, AND CALIFORNIAN TEC SAMPLES [35]

Parameters	Samples			
	Australian	Saudi	Peruvian	Californian
r_{hg}	0.750	0.450	0.350	0.000
ϑ_{hg}	0.010	0.010	0.050	0.040
ϑ_m	0.000	0.000	0.170	0.000
s_1	85.00	85.00	92.80	85.00
s_2	15.00	15.00	7.200	15.00
μ_p	0.000	0.000	50.00	50.00
μ_m	100.0	100.0	0.000	0.000
μ_c	0.000	0.000	50.00	50.00

The parameter r_{hg} corresponds to the ratio between the mass fraction of hematite to the total mass fraction of hematite and goethite represented by ϑ_{hg}. The parameter ϑ_m represents the mass fraction of magnetite. The texture of the samples is described by the percentages (%) of sand (s_1) and silt (s_2) particles. The particle type distributions considered in the simulations are given in terms of the percentages (%) of pure (μ_p), mixed (μ_m), and coated (μ_c) grains. It is assumed that magnetite appears as pure particles in sand soils characterized by the presence of this mineral [4], [38].

consisted in computer simulations to assess the effects of variations in sand-grain morphology on the visible and near-infrared spectral signature of sandy landscapes characterized by distinct iron-oxide distribution patterns.

V. RESULTS AND DISCUSSION

Initially, we performed simulations to verify the influence of particle size on the reflectance of the sand samples. The results of these simulations presented in Fig. 6 are in agreement with experimental observations [10] as well as theoretical investigations [7], [9] reported in the literature showing that grain size increases lead to reflectance decreases. These simulation results, albeit not the main focus of our investigation, confirmed the predictive capabilities of our *in silico* experimental framework.

We then proceeded to the simulations involving roundness and sphericity variations, the central component of our investigation. The results of these simulations presented in Figs. 7 and 8 suggest that the reflectance of sand soils is sensitive to variations

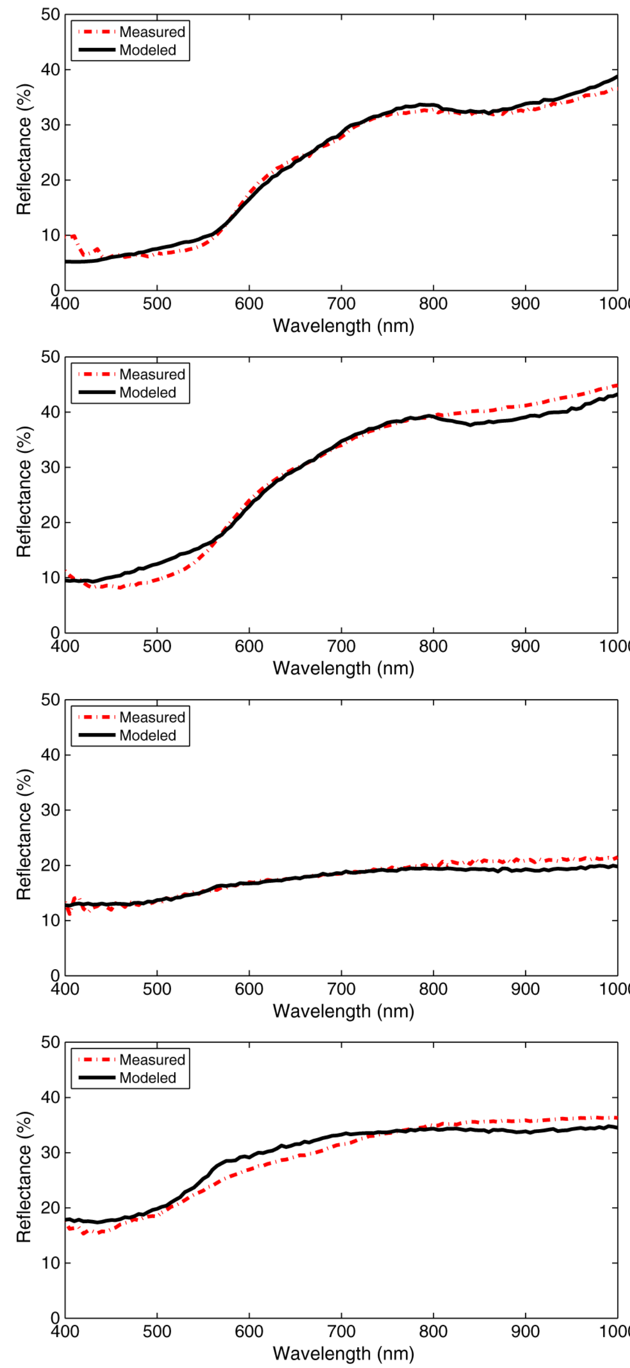

Fig. 5. Measured and modeled reflectance curves for the four sand samples employed in this investigation. From top to bottom: Australian, Saudi, Peruvian, and Californian samples. Measured curves are provided in the U.S. Army Topographic Engineering Center (TEC) database [35]. These samples are originally from a red (hematite-rich) dune in Australia (TEC #10019201), a dune in Saudi Arabia (TEC #13j9823), a magnetite-rich site in Peru (TEC #10039240), and a dike outcrop in California (TEC #19au9815). The modeled curves were obtained using the SPLITS model [29], [32] and the sand characterization data provided in Tables I–III.

in the sand-grain shape, and this sensitivity tends to be higher in spectral regions characterized by higher reflectance values, i.e., toward the end of the visible spectrum and the near-infrared domain where the extinction coefficients of the iron oxides have lower values [41]–[43]. These results also suggest that the spectral signature of sand soils tend to be less sensitive to

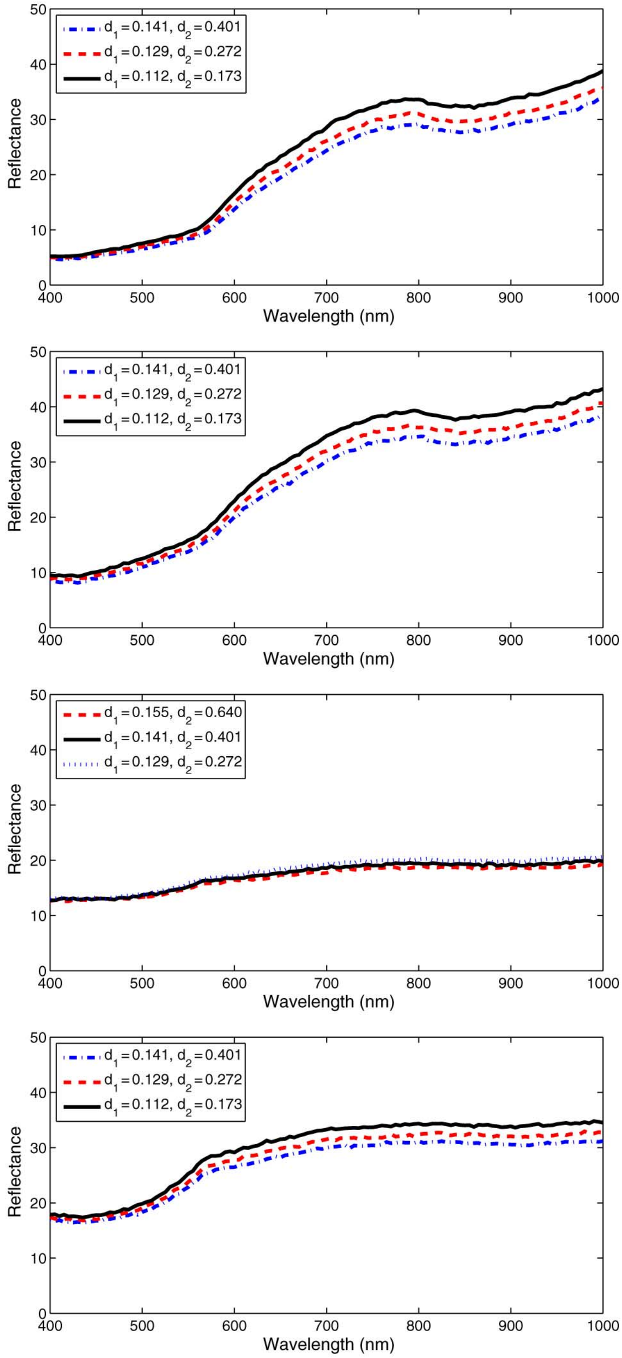

Fig. 6. Simulations of reflectance changes associated with changes in the size of the sand-sized and silt-sized particles. From top to bottom: Australian, Saudi, Peruvian, and Californian samples. Size variations are accounted for in terms of their geometric mean particle diameters (d_1 and d_2, respectively, given in mm) as listed in Table II. The solid lines correspond to the baseline reflectance curves computed using the data depicted in Table III.

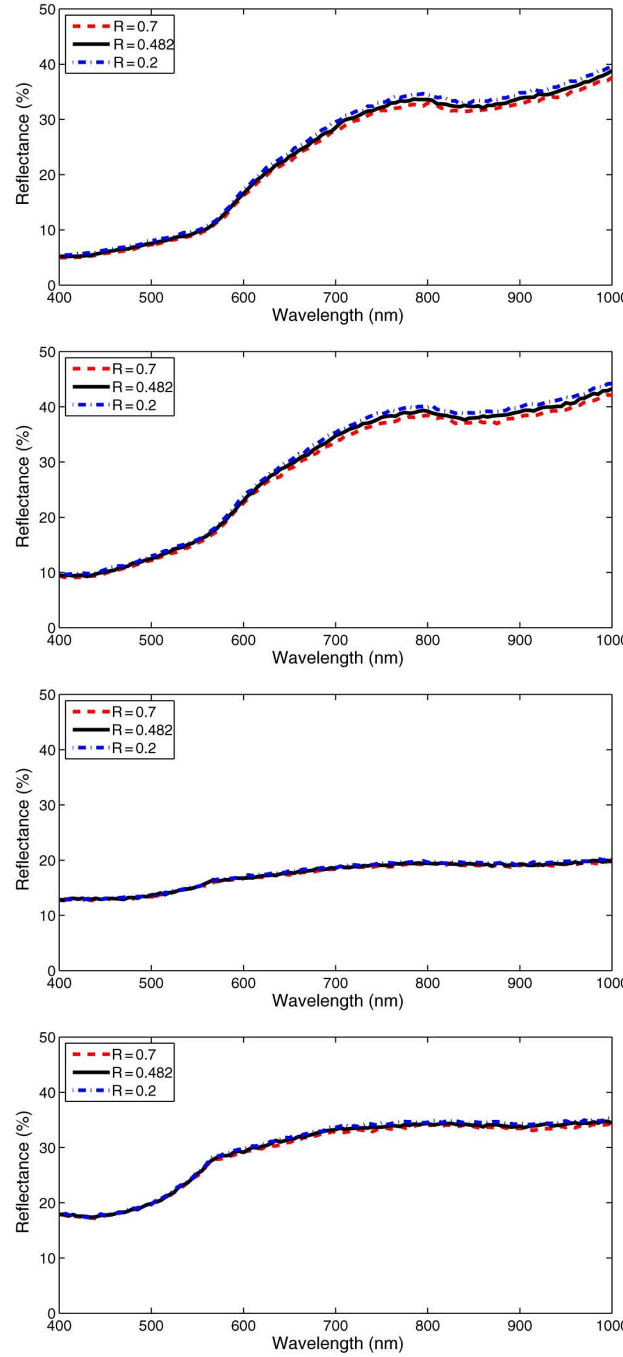

Fig. 7. Simulations of reflectance changes associated with minimum, maximum, and mean roundness (R) values provided in Table I. From top to bottom: Australian, Saudi, Peruvian, and Californian samples. The solid lines correspond to the baseline reflectance curves computed using the data depicted in Table III.

variations in roundness (Fig. 7) than to variations in sphericity (Fig. 8).

The more prominent impact of sphericity observed in our *in silico* experiments is consistent with the fact sphericity variations tend to have a more substantial influence on the probability of light absorption by the grains, which, in turn, has a larger impact in the overall reflectance of sand soils [6], [10]. Such an influence on light absorption is associated with changes in the path length of light travelling within the sand grains and their coatings [29]. Roundness variations, on the other hand, tend to have a more substantial influence on the spatial distribution of light reflected by surface features associated with the large-scale roughness of the sand grains [17], [18].

Besides these quantitative differences, our *in silico* experiments also indicate significant qualitative differences in the effects of roundness and sphericity on the visible and near-infrared spectral signature of sand soils. More specifically, reflectance changes associated with increased roundness tend to be independent on how the iron oxide particles are distributed

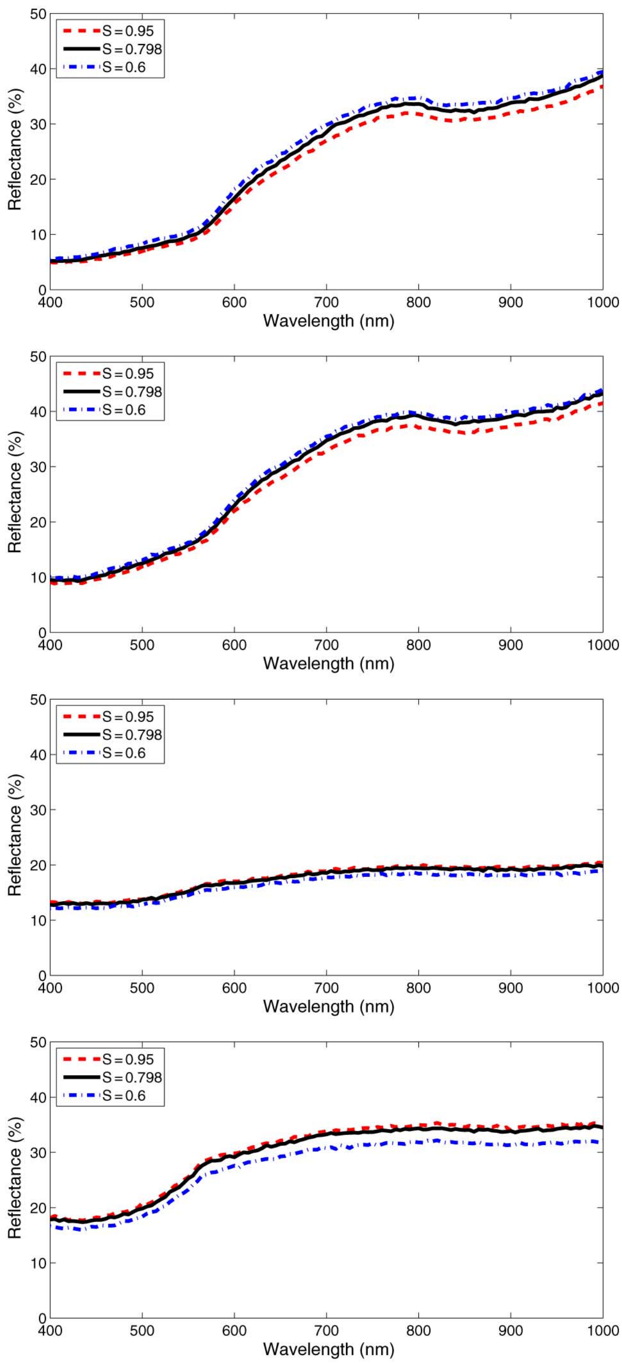

Fig. 8. Simulations of reflectance changes associated with minimum, maximum, and mean sphericity (S) values provided in Table I. From top to bottom: Australian, Saudi, Peruvian, and Californian samples. The solid lines correspond to the baseline reflectance curves computed using the data depicted in Table III.

within the sand samples (Fig. 7), with a roundness increase leading to a minor reflectance decrease. Reflectance changes associated with sphericity variations, however, may depend on the distribution patterns of these minerals (Fig. 8). We remark that the iron oxides may be present in pure form, mixed with the parent material or as a coating formed on the sand grains. Accordingly, examining the sphericity experiments more closely, one can note that the reflectance of a sand sample may decrease with increased sphericity when the iron oxides are mixed with the parent material (Fig. 8, two top graphs). However, one can also note that it may increase with increased sphericity when the iron oxides are distributed in pure form or as coatings (Fig. 8, two bottom graphs).

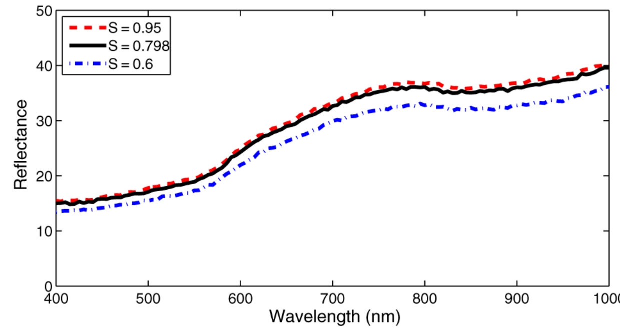

Fig. 9. Modeled reflectance curves for a modified Australian sand sample obtained considering the minimum, maximum, and mean sphericity (S) values provided in Table I. For this modified sample, the particle type distribution employed in the simulation of the Australian sample ($\mu_p = 0$, $\mu_m = 100$, and $\mu_c = 0$ given in Table III) was replaced by the particle type distribution employed in the simulation of the Peruvian and Californian sample ($\mu_p = 50$, $\mu_m = 0$, and $\mu_c = 50$ given in Table III).

In order to further assess the influence of particle type distribution and mitigate any bias from considering samples with different iron-oxide contents, we performed two additional sets of simulations. In the first one, we considered a modified Australian sand sample with the same particle type distribution employed in the Peruvian and Californian samples ($\mu_p = 50$, $\mu_m = 0$, and $\mu_c = 50$ given in Table III). We then computed its reflectance curves associated with the minimum, maximum, and mean sphericity values given in Table I. The results presented in Fig. 9 show a sphericity increase leading to a reflectance increase, i.e., the same behaviour observed for the Peruvian and Californian samples (Fig. 8, two bottom graphs) which have distinct iron-oxide contents, but the same iron-oxide distribution pattern (particle type distribution) employed in the modified Australian sample.

In the second set of additional simulations, we considered a modified Californian sand sample with the same particle type distribution employed in the Australian and Saudi samples ($\mu_p = 0$, $\mu_m = 100$, and $\mu_c = 0$ given in Table III). Again, we computed the reflectance curves for this sample considering the minimum, maximum, and mean sphericity values given in Table I. The results presented in Fig. 10 show a sphericity increase leading to a reflectance decrease, i.e., the same behaviour observed for the Australian and Saudi samples (Fig. 8, two top graphs) with distinct iron-oxide contents, but with the same iron-oxide distribution pattern (particle type distribution) employed in the modified Californian sample. Hence, the results presented in Figs. 9 and 10 further indicate that reflectance tends to decrease with increased sphericity when the iron oxides are mixed with the parent material, and increase with increased sphericity when the iron oxides are distributed as pure or coated particles, regardless of the dominant form of iron-oxide present in the samples.

In summary, our simulations demonstrate that not only the size, but also the shape of sand grains can have noticeable effects on the reflectance of sand soils. In fact, our simulations show that the representation of sand grains by spheres may lead to

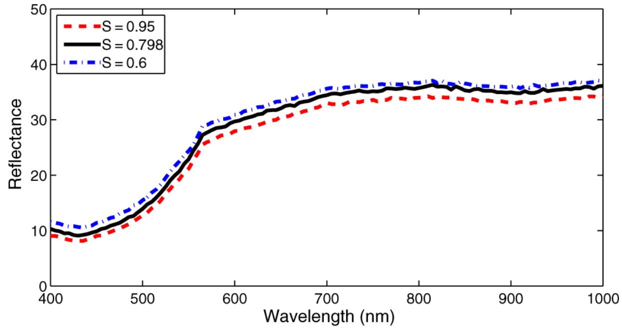

Fig. 10. Modeled reflectance curves for a modified Californian sand sample obtained considering the minimum, maximum, and mean sphericity (S) values provided in Table I. For this modified sample, the particle type distribution employed in the simulation of the Californian sample ($\mu_p = 50$, $\mu_m = 0$, and $\mu_c = 50$ given in Table III) was replaced by the particle type distribution employed in simulation of the Australian and Saudi sample ($\mu_p = 0$, $\mu_m = 100$, and $\mu_c = 0$ given in Table III).

significant deviations from the actual spectral signature of sand soils. We remark that while a sphere has sphericity and roundness equal to 1, actual sand particles have sphericity and roundness values markedly distinct from 1. Moreover, although both sphericity and roundness contribute to these effects, the former can have a more substantial influence on the visible and near-infrared reflectance of sand soils.

Our *in silico* experiments also indicate that the influence of sphericity may vary depending on how the iron oxides are distributed within the sand soils. Since the shape of sand grains and the distribution patterns of iron oxides (in pure form, mixed, or as contaminants) are directly connected with the geomorphology of sandy landscapes, their interplay needs to be carefully taken into account in the development of new soil investigation methodologies, particularly those based on the integration of remote sensing data with predictive computer modeling.

Finally, it is important to note that the influence of sand-grain morphology on the reflectance of sand soils can be significantly masked by the presence of water and organic matter. We remark, however, that our investigation focused on sand samples whose water and organic matter contents can be considered negligible. We also remark that although a given sand soil may be completely depleted of water and organic matter in their current deposition stage, these materials may have participated in its formation process. As a result, these materials, notably water, may have left clues of their earlier presence imprinted on the morphology of its constituent grains [3], [4], [14]. Viewed in this context, we highlight that reflectance variations associated with distinct grain shape properties, albeit less pronounced than those elicited by water and organic matter, should not be overlooked. Furthermore, while reflectance variations caused by the presence of water and organic matter are monotonic [10], [44], reflectance variations associated with distinct grain shape properties can present distinct qualitative trends depending on the iron oxide contents and distribution patterns of a given soil as demonstrated in this work. Accordingly, we believe that the close examination of such spectral signature changes can potentially lead to new avenues of research involving the mineralogy and environmental history of terrestrial an extra-terrestrial sandy landscapes.

VI. Conclusion

In this paper, we have investigated the effects of sand-grain morphology on the visible and near-infrared reflectance of sand soils with different mineralogical characteristics. This investigation was performed using a predictive simulation framework supported by sand characterization data provided in the scientific literature. Using this framework, we performed controlled *in silico* experiments in which we assessed the interplay between key morphological properties (size, roundness, and sphericity) and mineralogical characteristics (iron-oxide content and particle type distribution) with respect to the spectral signature of sand soils.

Although *in situ* experiments are required to assess the full applicability of our findings, we believe that they provide a sound basis for future investigations in this area. To allow the full reproduction and extension of our *in silico* experiments, we made the light transport model (SPLITS) and the sand characterization data employed in this work openly available for online use [32].

As future work, we plan to investigate the effects of soil porosity on the spectral signature of sandy landscapes under different illumination and moisture conditions. Moreover, we believe that the interdisciplinary research methodologies can result in significant advances not only in the retrieval of texture and mineralogical information from sand soils, but also in the current understanding of the origins of terrestrial and extraterrestrial sandy landscapes. Therefore, we also intend to enable the extension of our investigations to extraterrestrial sand soils by incorporating to our online simulation set-up their specific mineralogical characteristics such as the presence of different parent materials (e.g., basalt found in Martian sands [22]).

Acknowledgments

The authors would like to thank the anonymous reviewers for their helpful comments and criticisms.

References

[1] D. C. Catling and J. M. Moore, "The nature of coarse-grained crystalline hematite and its implications for the early environment of Mars," *Icarus*, vol. 165, pp. 277–300, 2003.

[2] A. Mottana, R. Crespi, and G. Liborio, *Simon and Schuster's Guide to Rocks and Minerals*, New York, NY, USA: Simon and Schuster, Inc., 1978.

[3] H. Wopfner and C. R. Twidale, "Australian desert dunes: Wind rift or depositional origin?," *Austral. J. Earth Sci.*, vol. 48, pp. 239–244, 2001.

[4] K. S. Edgett and N. Lancaster, "Volcaniclastic aeolian dunes: Terrestrial examples and applications to Martian sands," *J. Arid Environ.*, vol. 25, pp. 271–297, 1993.

[5] K. R. Kuhlman, J. Marshall, N. D. Evans, and A. Luttge, "Australian red dune sand: A potential Martian regolith analog," in *Proc. Workshop Martian Highlands Mojave Desert Analogs*, Barstow, CA, USA, 2001, pp. 4021–4022.

[6] J. E. Bullard and K. White, "Quantifying iron oxide coatings on dune sands using spectrometric measurements: An example from the Simpson–Strzelecki desert, Australia," *J. Geophys. Res.*, vol. 107, no. B6, pp. 1–11, 2002.

[7] G. S. Okin and T. H. Painter, "Effect of grain size on remotely sensed spectral reflectance of sandy desert surfaces," *Remote Sens. Environ.*, vol. 89, pp. 272–280, 2004.

[8] C. H. Hugenholtz, N. Levin, T. E. Barchyn, and M. C. Baddock, "Remote sensing and spatial analysis of aeolian sand dunes: A review and outlook," *Earth Sci. Rev.*, vol. 111, pp. 319–334, 2012.

[9] D. J. Leu, "Visible and near-infrared reflectance of beach sands: A study on the spectral reflectance/grain size relationship," *Remote Sens. Environ.*, vol. 6, no. 3, pp. 169–182, 1977.

[10] M. F. Baumgardner, L. F. Silva, L. L. Biehl, and E. R. Stoner, "Reflectance properties of soils," *Adv. Agron.*, vol. 38, pp. 1–43, 1985.
[11] D. L. Neema, A. Shah, and A. N. Patel, "A statistical optical model for light reflection and penetration through sand," *Int. J. Remote Sens.*, vol. 8, no. 8, pp. 1209–1217, 1987.
[12] W. C. Krumbein, "Measurement and geological significance of shape and roundness of sedimentary particles," *J. Sediment. Petrol.*, vol. 11, no. 2, pp. 64–72, 1941.
[13] K. Seiferlin, P. Ehrenfreund, J. Garry, K. Gunderson, E. Hütter, G. Kargl, A. Maturilli, and J. P. Merrison, "Simulating Martian regolith in the laboratory," *Planet. Space Sci.*, vol. 56, pp. 2009–2025, 2008.
[14] H. Wadell, "Volume, shape, and roundness of rock particles," *J. Geol.*, vol. 40, no. 5, pp. 443–451, 1932.
[15] H. Wadell, "Sphericity and roundness of rock particles," *J. Geol.*, vol. 41, no. 3, pp. 310–331, 1933.
[16] H. Wadell, "Volume, shape, and roundness of quartz particles," *J. Geol.*, vol. 43, no. 3, pp. 250–280, 1935.
[17] P. J. Barret, "The shape of rock particles: A critical review," *Sedimentology*, vol. 27, pp. 291–303, 1980.
[18] E. T. Bowman, K. Soga, and T. W. Drumond, "Particle shape characterization using Fourier descriptor analysis," *Geotechnique*, vol. 51, pp. 1–43, 2001.
[19] K. Asumadu, R. J. Gilkes, H. M. Churchward, and T. M. Armitage, "Detailed characterization of quartz in two sandy soils, Western Australia," *Geoderma*, vol. 41, pp. 29–47, 1987.
[20] S. Zhang, D. B. Kent, D. C. Elbert, Z. Shi, J. A. Davis, and D. R. Veblen, "Mineralogy, morphology, and textural relationships in coatings on quartz grains sediments in a quartz-sand aquifer," *J. Contam. Hydrol.*, vol. 124, pp. 57–67, 2011.
[21] J. Marshall, K. R. Kuhlman, R. Stevens, and M. Meyyappan, "Study of a Martian aeolian sand analog with MECA spectroscopy," in *Proc. Annu. Lunar Planet. Sci. Conf.*, Houston, TX, USA, 2001, pp. 1265–1266.
[22] J. F. Kok, E. J. R. Parteli, T. I. Michaels, and D. B. Karam, "The physics of wind-blown sand and dust," *Rep. Progr. Phys.*, vol. 75, pp. 1–72, 2012.
[23] G. V. G. Baranoski, B. W. Kimmel, T. F. Chen, E. Miranda, and D. Yim, "Effects of sand grain shape on the spectral signature of sandy landscapes in the visible domain," in *Proc. 2013 IEEE Int. Geosci. Remote Sens. Symp.* (IGARSS), Melbourne, Australia, 2013, pp. 3060–3063.
[24] G. Cho, J. Dodds, and J. C. Santamarina, "Particle shape effects on packing density, stiffness, and strength: Natural and crushed sands," *J. Geotech. Geoenviron. Eng.*, vol. 132, pp. 591–602, 2006.
[25] M. A. Shirazi, L. Boersma, and J. W. Hart, "A unifying quantitative analysis of soil texture: Improvement of precision and extension of scale," *Soil Sci. Soc. Amer. J.*, vol. 52, no. 1, pp. 181–190, 1988.
[26] M. J. Vepraskas and D. K. Cassel, "Sphericity and roundness of sand in costal plain soils and relationships with soil physical properties," *Soil Sci. Soc. Amer. J.*, vol. 51, no. 5, pp. 1108–1112, 1987.
[27] N. Riley, "Projection sphericity," *J. Sediment. Petrol.*, vol. 11, pp. 94–95, 1941.
[28] A. J. L. M. Siang, D. C. Wijeyesekera, A. Zainorabidin, and I. Bakar, "The effects of particle morphology (shapes and sizes) characteristics on its engineering behaviour and sustainable engineering performance of sand," *Int. J. Integr. Eng.*, vol. 4, no. 3, pp. 27–37, 2012.
[29] B. W. Kimmel and G. V. G. Baranoski, "A novel approach for simulating light interaction with particulate materials: Application to the modeling of sand spectral properties," *Optic. Express*, vol. 15, no. 15, pp. 9755–9777, 2007.
[30] G. V. G. Baranoski, T. Dimson, T. F. Chen, B. W. Kimmel, D. Yim, and E. Miranda, "Rapid dissemination of light transport models on the web," *IEEE Comput. Graph. Appl.*, vol. 32, no. 3, pp. 10–15, May/Jun. 2012.
[31] B. W. Kimmel and G. V. G. Baranoski, "A compact framework to efficiently represent the reflectance of sand samples," *IEEE Trans. Geosci. Remote Sens.*, vol. 47, no. 11, pp. 3625–3629, Nov. 2009.
[32] Natural Phenomena Simulation Group (NPSG). (2012) *Run SPLITS Online*, School of Computer Science, University of Waterloo, ON, Canada [Online]. Available: http://www.npsg.uwaterloo.ca/models/splits.php.
[33] G. V. G. Baranoski, J. G. Rokne, and G. Xu, "Virtual spectrophotometric measurements for biologically and physically-based rendering," *Visual Comput.*, vol. 17, no. 8, pp. 506–518, 2001.
[34] B. W. Kimmel and G. V. G. Baranoski, "Simulating the appearance of sandy landscapes," *Comput. Graph.*, vol. 34, no. 4, pp. 441–448, 2010.
[35] J. N. Rinker, C. S. Breed, J. F. McCauley, and P. A. Corl, "Remote sensing field guide—Desert," U.S. Army Topographic Engineering Center, Fort Belvoir, VA, USA, Tech. Rep. ETL-0588, Sep. 1991.
[36] N. C. Brady, *The Nature and Properties of Soils*, 8th ed., New York, NY, USA: Macmillan Publishing Co., 1974.
[37] H. Wopfner and C. R. Twidale, "Formation and age of desert dunes in Lake Eyre depocentres in central Australia," *Geolog. Rundschau*, vol. 77, no. 3, pp. 815–834, 1988.
[38] G. R. Hunt, J. W. Salisbury, and C. J. Lenhoff, "Visible and near-infrared spectra of minerals and rocks: III oxides and hydroxides," *Modern Geol.*, vol. 2, no. 3, pp. 195–205, 1971.
[39] F. E. Nicodemus, J. C. Richmond, J. J. Hsia, I. W. Ginsberg, and T. Limperis, "Geometrical considerations and nomenclature for reflectance," in *Physics-Based Vision Principles Practice: Radiometry*, L. B. Wolff, S. A. Shafer, and G. E. Healey, Eds., Boston, MA, USA: Jones and Bartlett Publishers, 1992, pp. 94–145.
[40] S. Jacquemoud, S. L. Ustin, J. Verdebout, G. Schmuck, G. Andreoli, and B. Hosgood, "Estimating leaf biochemistry using PROSPECT leaf optical properties model," *Remote Sens. Environ.*, vol. 56, pp. 194–202, 1996.
[41] A. Schlegel, S. F. Alvarado, and P. Wachter, "Optical properties of magnetite (Fe_3O_4)," *J. Phys. C: Solid State Phys.*, vol. 12, pp. 1157–1164, 1979.
[42] I. N. Sokolik and O. B. Toon, "Incorporation of mineralogical composition into models of the radiative properties of mineral aerosol from UV to IR wavelengths," *J. Geophys. Res.*, vol. 104, no. D8, pp. 9423–9444, 1999.
[43] W. G. Eagan and T. W. Hilgeman, *Optical Properties of Inhomogeneous Materials*, New York, NY, USA: Academic Press, 1979.
[44] C. Atzberger, "Soil optical properties—A review," Remote Sens. Dept., Univ. Trier, Trier, Germany, Tech. Rep. D-54286, 2002.

Gladimir V. G. Baranoski (SM'07) received the Ph.D. degree in computer science from the University of Calgary, Calgary, Alberta, Canada, in 1998.

In 2001, he became a Faculty Member of the David R. Cheriton School of Computer Science at the University of Waterloo, Waterloo, Canada. His current research interests include the predictive simulation of light interactions with natural materials and the biophysically based rendering of natural phenomena. Due to his interdisciplinary research activities, Prof. Baranoski has established the Natural Phenomena Simulation Group (NPSG) that carries on research projects with theoretical and practical applications in a wide range of fields, from computer graphics and computational mathematics to tissue optics and remote sensing.

After completing his doctorate, he was awarded a 2-year Postdoctoral Fellowship from the National Sciences and Research Council of Canada (NSERC).

Bradley W. Kimmel received the Bachelor's degree in pure mathematics and computer science and the M. Math. degree in computer science from the University of Waterloo, Waterloo, Canada, in 2002 and 2006, respectively. He is currently working toward the Ph.D. degree in computer science with the Natural Phenomena Simulation Group, David R. Cheriton School of Computer Science, Waterloo, Canada.

His research interests include simulating light interactions with natural environments.

T. Francis Chen received the Bachelor's and Master's degrees in computer science from the University of Waterloo,Waterloo, Canada, in 2006 and 2009, respectively. He is currently a doctoral candidate in the Natural Phenomena Simulation Group at the University of Waterloo.

His primary interest is in the predictive simulation of how light interacts with organic and inorganic materials.

Erik Miranda received the B.S.E. (Bachelor of Software Engineering) degree at the University of Waterloo, Waterloo, Canada, in 2010. He is currently pursuing a M.Math. degree in computer science with the Natural Phenomena Simulation Group, David R. Cheriton School of Computer Science also at the University of Waterloo.

His primary research interests focus on the application of computer graphics techniques for acoustic propagation.